UNIVERSIDADE FEDERAL DO PARA

INSTITUTO DE GEOCIÊNCIAS

FACULDADE DE GEOFÍSICA

ESTIMATIVA DE ORIENTAÇÃO DE FRATURAS EM MEIOS ANISOTRÓPICOS UTILIZANDO ONDAS CISALHANTES: UMA ABORDAGEM EXPERIMENTAL

LÉO KIRCHHOF SANTOS

Belém

2014

LÉO KIRCHHOF SANTOS

ESTIMATIVA DE ORIENTAÇÃO DE FRATURAS EM MEIOS ANISOTRÓPICOS UTILIZANDO ONDAS CISALHANTES: UMA ABORDAGEM EXPERIMENTAL

Trabalho de Conclusão de Curso apresentado à Faculdade de Geofísica da Universidade Federal do Pará-UFPA, em cumprimento às. exigências para obtenção de grau de bacharel em Geofísica

Orientador: Prof. Dr. José Jadsom Sampaio de Figueiredo

BELÉM

2014

Dados Internacionais de Catalogação-na-Publicação (CIP)
Biblioteca Geólogo Raimundo Montenegro Garcia de Montalvão

S237e Santos, Léo Kirchhof

Estimativa de orientação de fraturas em meios anisotrópicos utilizando ondas cisalhantes: uma abordagem experimental. / Léo Kirchhof Santos. – 2014

52 f. : il.

Orientador: José Jadsom Sampaio de Figueiredo

Trabalho de Conclusão de Curso (graduação) - Universidade Federal do Pará, Instituto de Geociências, Faculdade de Geofísica, Belém, 2014.

1. Anisotropia. 2. Ondas Cisalhantes. Modelagem Física Sísmica. Orientação de Fraturas. I. Título.

CDD 22. ed.: 552.06

LÉO KIRCHHOF SANTOS

Estimativa de orientação de fraturas em meios anisotrópicos utilizando ondas cisalhantes: uma abordagem experimental

Trabalho de Conclusão de Curso apresentado à Faculdade de Geofísica da Universidade Federal do Pará-UFPA, em cumprimento às exigências para obtenção de grau de bacharel em Geofísica.

Data de aprovação: 17/01/2014

Conceito: Excelente

Banca Examinadora:

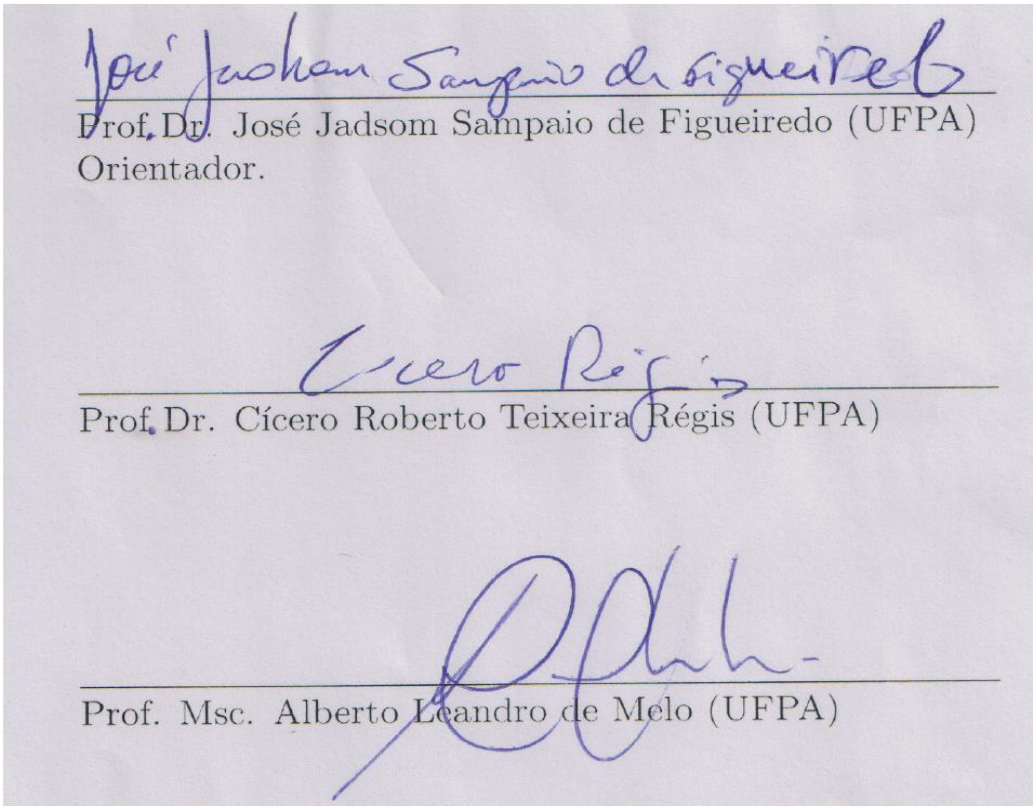

Prof. Dr. José Jadsom Sampaio de Figueiredo (UFPA)
Orientador.

Prof. Dr. Cícero Roberto Teixeira Régis (UFPA)

Prof. Msc. Alberto Leandro de Melo (UFPA)

AGRADECIMENTOS

À minha família, em especial à minha mãe, Laudia, principal responsável por todos os momentos mais importantes da minha vida.

À minha namorada Fabiana pelos momentos passados ao meu lado e pela ajuda em vários momentos difíceis.

Ao meu Orientador Prof. Dr. Jadsom José de Figueiredo por todo suporte oferecido para a confecção desse trabalho e por todo conhecimento que me passou e tem me passado.

Ao Prof. Dr. Cícero Roberto Teixeira Régis e ao Prof. Msc. Alberto Leandro de Melo por terem aceitado participar da banca examinadora.

Aos meus verdadeiros amigos, peças fundamentais para minha construção como ser humano.

RESUMO

A propagação da onda S em um meio anisotrópico fraturado pode fornecer informações valiosas sobre a orientação de fraturas em um meio. O principal objetivo deste trabalho é recuperar informação sobre a orientação de fraturas baseado na análise de onda S. Para isso, medidas ultrassônicas de onda S foram conduzidas em um modelo físico sintético feito de resina epoxi (matriz isotrópica) contendo pequenas tiras de borracha (fraturas artificiais) inseridas no interior da resina com o objetivo de simular um meio anisotrópico homogêneo. Nesta abordagem, foi usado fontes de baixa frequência, frequência intermediária e alta frequência, com 90, 431 e 840 kHz, respectivamente. Integrando a análise de sismogramas de onda S, painéis de correlação cruzada e curvas do parâmetro de Thomsen, foi possível estimar a orientação das fraturas em um meio com diferentes zonas fraturadas. Informação adicional sobre a direção das fraturas foi obtida a partir de picos associados a onda S espalhada. Isso foi possível usando resultados de curvas de frequência em função do ângulo de polarização da onda S. Além disso, um processo de filtragem utilizando filtro passa banda foi realizado nos sismogramas de frequências intermediaria e alta com o objetivo de obter sismogramas de baixa frequência. Análise de espectros de frequência-número de onda (FK) foi feita para auxiliar esse processo de filtragem. Os resultados obtidos usando correlação cruzada e parâmetro γ a partir de dados filtrados foram similares aos resultados obtidos usando fonte de baixa frequência. Isso destacou a possibilidade de usar fontes de baixo custo (alta frequência) para recuperar sinais com baixa frequência sem uma grande perda de informação sobre tempo de trânsito.

Palavras-chaves: Anisotropia. Ondas Cisalhantes. Modelagem Física Sísmica. Orientação de Fraturas.

ABSTRACT

Shear-wave propagation in anisotropic fractured/cracked media can provide valuable information about fracture swarm orientations. The main goal of this work is to recover information about fracture orientation based on the S-waveforms. For this study, ultrasonic measurements of S-waves in a synthetic physical model made of resin epoxy (isotropic matrix) with small rubber strips (artificial cracks) inserted in it to simulate a homogeneous anisotropic media. In this approach, it is used low, intermediate and high frequency shear-wave sources, with 90, 431 and 840 kHz, respectively. Integrating the S-wave seismograms, cross-correlation panels and the anisotropic parameter curves analysis, it was possible to estimate crack orientation in single fracture zones. Additional information was obtained from the high frequency peaks associated to scattered S-waves. This was possible using results from frequency versus angle of polarization curves. Moreover, a bandpass filtering process was performed in the intermediate and high frequencies seismograms in order to obtain low frequency seismograms. Spectral analysis from frequency-wavenumber (F-K) spectra was performed to support this filtering process. The results obtained using cross-correlation and parameter γ from filtered data were quite similar to those obtained using low frequency source. This highlighted the possibility of using cheap high frequency sources to recover signals at low frequency range without losing traveltime information.

Keywords: Anisotropy. Shear-waves. Seismic Physical Modeling. Fracture Orientation.

LIST OF ILLUSTRATIONS

LIST OF TABLES

CONTENTS

1 INTRODUCTION

Knowledge about the features of fractures in a reservoir is very important to optimize the production of fluids. In certain reservoirs, the oil and gas production is controlled by fractures of the subsurface. Location, orientation and fracture density are important parameters to be characterized. Some fractured reservoirs (i.e. shale and carbonates) use to have high secondary porosity, however their permeability is usually low (LONERGAN, 2007; NELSON, 2001). This permeability can be increased by the hydraulic fracturing process and knowing the preferential orientation of the fractures before this process is important to enhance the fluid flow (HOLDITCH et al., 1978). Figure 1.1 illustrates a real anisotropic media with variable fracture orientations within a given fracture swarm.

Due to the importance of fracture characterization, several methods have been developed in order to obtain information about fracture parameters. Using a parameter called “scattering index" in high frequency domain, Willis et al. (2005) were able to estimate the preferential orientation of a set of fractures from the analysis of backscattered energy. A satisfactory result was obtained on a real field dataset. Zhang et al. (2006) also estimated the fracture spacing using backscattered energy, but their analysis was based on the Local Wave field Decomposition (LWD) method proposed by Sacchi et al. (2004). Using a seismic section in the time-domain, generated from a shot gather normal to the fracture strike, LWD was used to characterize the coherent energy reflected from fractures. Once characterized, a new seismic section was generated showing only the contribution of fracture reflections. From this new seismic section, an F-K panel was created, from which they extracted the highest wavenumber value. This value was then used to estimate the fracture spacing. The method had a suitable result and was also used on a real situation.

It is well known that the lack of real anisotropic dataset is a common issue on testing methods. One of the alternatives to overcome this issue is to use physical modeling experiments. Based on Hudson (1981) theory's, Tillotson et al. (2012) used a synthetic silica cemented sandstone to define the relationship between the shear-wave splitting (which is a function of S1 and S2 velocities) and the fracture density of this synthetic rock. Their results showed that the shear-wave splitting has the same order of the fracture density, unconstraining the saturating fluid. This relationship was also confirmed by previous experiments performed by Assad et al. (1992) using a synthetic anisotropic medium made of resin epoxy with penny-shaped rubber inclusions.

From analysis of the seismograms (created by low frequency sources), cross-correlation panels γ and anisotropy parameter curves, Figueiredo, Schleicher e Stewart (2012) estimated the preferential fracture set orientation of each region in a synthetic model. This work complements Figueiredo, Schleicher e Stewart. (op.cit.)'s research on estimating fracture orientation. While the previous work of Figueiredo, Schleicher e Stewart (op.cit.) used only low frequency sources to obtain information about preferential fracture orientation in the model, this approach uses three different frequency sources to achieve this. The sources are in low (LF), intermediate (IF) and high frequency (HF) with 90, 431 and 840 kHz, respectively. In order to recover reliable information from these higher frequencies, it is realized a bandpass filtering process to obtain low frequency seismograms. Before the filtering process, the seismograms are converted into F-K spectra in order to visualize the frequency distribution of signals.

The analysis performed by Figueiredo, Schleicher e Stewart (op.cit.) was efficient on extracting fracture orientation information when the S-wave propagation was normal to the bedding planes. Here their analyses are extended to obtain information about fracture orientation when S-wave propagation is parallel to the bedding planes. The first step in this work is the interpretation based on seismograms, high coherence value of correlograms and anisotropy parameter curves for both original and filtered datasets. Then, it is estimated the orientation of fractures from frequency versus angle of polarization curves, generated after the Fourier transform of high frequency seismograms. Similar to Figueiredo, Schleicher e Stewart (op.cit.), the interpretation also considers the fracture orientation as an unknown parameter. However, as a main assumption to the interpretation, the parameters, such as the size of the inclusions and the crack density, are considered as known.

Figure 1.1 – Fractured sandstone from Arches National Monument showing orthorhombic (top) and monoclinic (bottom) symmetries

Source: Far, Sayers e Thomsen (2013)

2 EXPERIMENTAL PROCEDURE

The construction of the anisotropic cracked sample as well as the ultrasonic measurements was carried out at the Allied Geophysical Laboratories (AGL) at the University of Houston, Texas. The experimental setup used to make samples and S-waveform measurements was the same used at previous works published by Omoboya et al. (2011); Figueiredo, Schleicher e Stewart (2012); Stewart et al. (2013); Figueiredo, Schleicher e Stewart (2013).

2.1 Sample preparation

Under controlled conditions, a cracked sample (M) with three different crack set orientations and approximated crack densities was constructed. A sample (R) without inclusions was also made in order to set reference results. Pictures of all samples are shown in Figure 2.1. Sample M has three different regions, but five different positions used for measurements, labeled 1 to 5 in Figure 2.1 a. Positions 2 and 4 are at the boundaries between the three different crack orientations. The isotropic sample R consisted of a single cast of epoxy resin. The cracked samples were constituted one layer at a time, with short intervals to allow for the introduction of the rubber cracks. To reduce possible boundary effects to a minimum, the interval between separated layers was kept as short as possible. A constant layer thickness of 0.5 cm for M was ensured by using the same volume of epoxy resin poured for each layer. After each layer with inclusions was added to the sample, air was extracted using a vacuum pump to avoid air bubbles in the epoxy resin. The solid rubber material used to simulate the cracks in the sample M was neoprene rubber. The ratio of compressional wave velocity between solid epoxy and neoprene was ~ 1.5. The S-wave velocity in rubber was difficult to determine because of the low shear modulus of this material. The wavelengths for body waves propagating in the model were in the range of 1.9-2.5 cm for P waves and 1.0-1.4 cm for S waves. The geometrical parameters of the included rubber-strip cracks in the cracked model are displayed in Table 2.1.

The crack density ϵ_C shown in Table 2.1 for cracked sample was estimated according to the Hudson (1981) formula,

$$\epsilon_C = \frac{NV_C}{V} = \frac{Nlh^2}{V}, \tag{2.1}$$

where N is the number of cracks, V_C is the volume of a single crack, and V is the volume of the model. For the strip-shaped cracks, $V_C = lh^2$, where l is the crack length and h is the crack aperture.

Table 2.1 – Geometrical parameters of the reference model (R) and the three regions (M-1, M-3, M5) of the cracked model

Model	Crack density (%)	Measuring length model (cm) L_Z	L_Y	Number of layers	Cracks per layer	Crack length(cm)	Crack aper.(cm)
R	Isotropic	7.51	7.62	0	0	-	-
M-1	4.5	7.56	7.89	10	36	0.8	0.2
M-3	4.5	7.56	7.89	10	36	0.8	0.2
M-5	4.5	7.59	7.81	10	36	0.8	0.2

Source: Figueiredo, Schleicher e Stewart (2012)

2.2 Ultrasonic measurement setup

Over these models, ultrasonic measurements using the Ultrasonic Research System at AGL with a pulse transmission technique were performed. The ultrasonic measurement system includes a pulser/receiver 5077PR, a digital oscilloscope, low-noise preamplifiers and P- and S-wave transducers with central frequencies at 90 kHz, 431 kHz and 840 kHz respectively. Fourier spectra for S-wave source signatures are shown at Figure 2.2. The sampling rate per channel for all experiments was 0.1 µs. There is a delay of 2.7 µs for all S-wave transducers. For the velocity computations, the scaled delay time was subtracted from the observed arrival time. The time-picking accuracy was ±0.2 µs, which yields an error in the estimated velocities of about ±4 m/s.

The device used to record the polarized S-wave seismograms is the same as the one depicted in Figueiredo, Schleicher e Stewart (2013). It was devised to allow a rotation of the source and receiver transducers, which were arranged on opposing sides of the model, separated by the measuring length (see Table 2.1). The initial shear-wave polarization was parallel to the X direction (Figure 2.1c) for both recordings in the Z and Y directions. To achieve changes in polarization, the transducers (source and receiver) were rotated 18 times,

by 10° at a time (i.e., 0° to 180°), until polarization was again parallel to the X direction, for both cases of S-wave propagation in the XY or XZ planes (see Figure 2.1b). Each of the 19 output traces was acquired with a 20-fold stack to eliminate ambient noise.

Table 2.2 – Physical parameters of transducers used to record S-wave seismograms in the samples depicted in Figure 2.1

Transducer Frequency	Catalogue Number	Transducer Diameter	Ricker Wavelet	Near Field Distance
90 kHz	V1548	25 mm	$(-t^3+3t)e^{\frac{t^2}{2}}$	~ 1.0 cm
431 kHz	V151-RB	25 mm	$(t^2-t-1)e^{\frac{t^2}{2}}$	~ 5.7 cm
840 kHz	V153-RB	13 mm	$(t^2-t-1)e^{\frac{t^2}{2}}$	~ 3.2 cm

Source: Figueiredo, Schleicher e Stewart (2013)

Figure 2.1 – (a) Photograph of the fractured model showing three regions with the same crack density but with three different set orientations. (b) Schematic diagram of crack placement of YX (bedding plane) and ZX planes of the fracture model. (c) Schematic representation of the S-wave transducer placing at the centers of opposite sides of the model

(a)

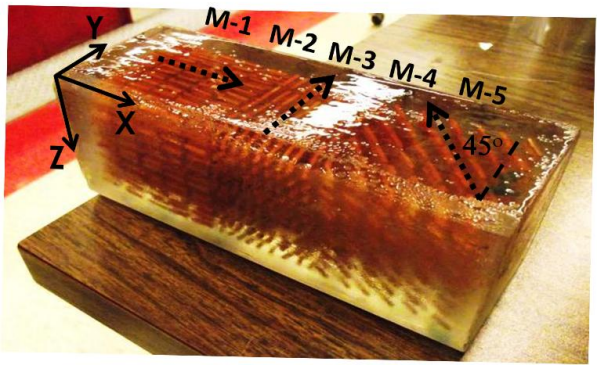

(b)

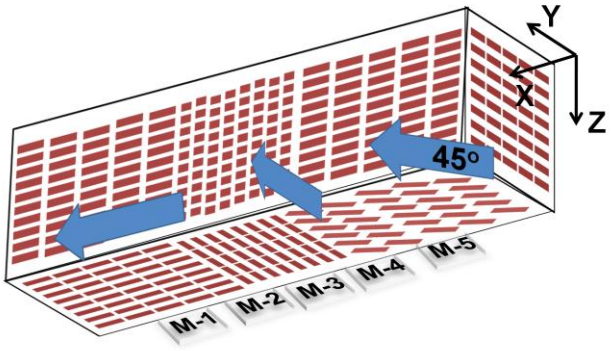

(c)

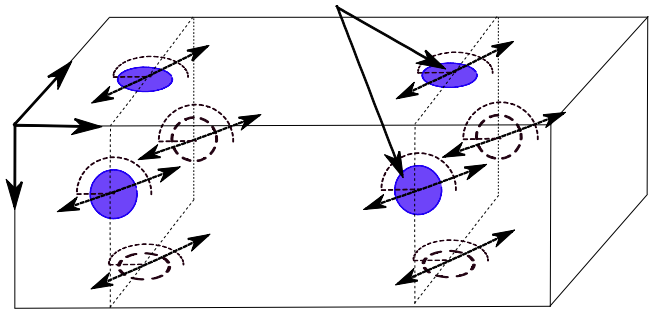

Source: Figueiredo, Schleicher e Stewart (2012)

Figure 2.2 – (a) The time domain, S-wave source signatures of the three transducers: LF = 90 kHz, IF = 431 kHz and HF = 840 kHz. (b) Fourier transform of each signature trace. (c) Fourier transform after Gaussian nonlinear fit. Here the dominant frequencies have become 89 kHz, 386 kHz and 805 kHz

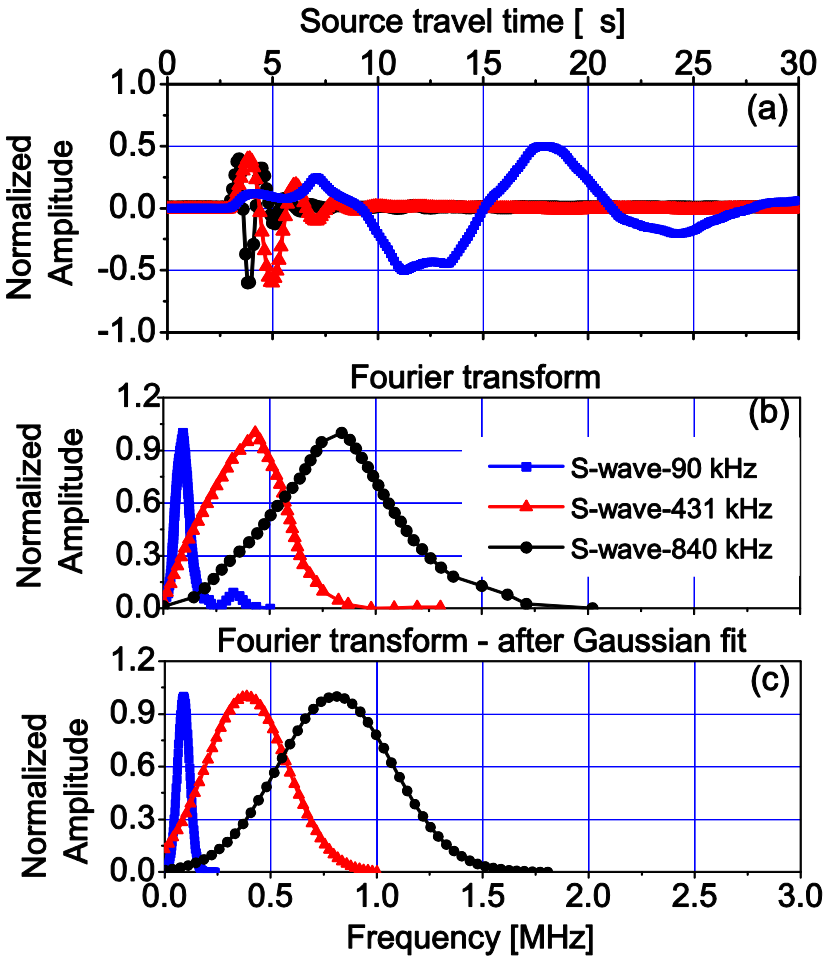

Source: Figueiredo, Schleicher e Stewart (2013)

3 RESULTS

In this section, it is presented the experimental results. The analyses are based on the two S-wave phases, fast S-wave (*S1*) and slow S-wave (*S2*). These phases are generated when the S-wave enters in an anisotropic medium, in this case a synthetic cracked sample, and separates itself in these two phases. This process is called S-wave splitting. The models used are one cracked sample with three different set of crack orientation and one uncracked sample that was used for reference. In a fractured medium, the S1 is always parallel to the fractures, while the S2 is always perpendicular to them. Besides the seismograms, it is also shown the analysis related to three seismic attributes: correlograms, parameter curves and frequency versus angle of polarization curves. Other results depicted here are related to frequency/FK spectral content in three different frequency ranges (LF, IF and HF).

3.1 S-wave seismograms

The Figure 3.1 shows the seismograms for LF, IF and HF for S-wave propagation in Z direction. Figure 3.2 shows the seismograms for LF, IF and HF for S-wave propagation in Y direction. The Figure 3.3 shows the seismograms for LF, IF (filtered) and HF (filtered) for S-wave propagation in Z direction. Figure 3.4 shows the seismograms for LF, IF (filtered) and HF (filtered) for S-wave propagation in Y direction. For LF seismograms of region M-1 as well as for S-wave propagation in both Z and Y directions, the minimum lag ($\Delta t = t(S2) - t(S1)$) occurs at 90°. This indicates the lowest S-wave velocity at 90°, making it possible to infer that the fractures are oriented parallel to the X direction. For region M-3, related to S-wave propagation in Z direction, the highest time lag is perpendicular to the time lag of region M-1. In other words, regions M-1 and M-3 are perpendicular to each other. More details about seismograms interpretation is depicted at Discussion section.

3.2 Spectrograms

The spectrograms were generated from F-K transform, which is the Fourier transform of a space-time domain signal. They show the frequency distribution of a signal and have an important role in noise reduction, avoiding spatial aliasing and estimating fracture spacing (ZHANG et al., 2006). The spectrograms depicted in Figures 3.5 and 3.6 are related to the

seismograms of Figures 3.1, 3.2, 3.3 and 3.4. First row of each Figure represents the spectrograms of the isotropic model. They approximately represent the original spectra of the transducers, since there is no significant frequency attenuation in the reference model.

Figure 3.1 – S-wave seismograms for LF, IF and HF sources, as a function of change in polarization from 0° to 180°, related to propagation in Z direction. The first row corresponds to the reference (R) sample and the other rows in descending order are the seismograms for positions M-1, M-2, M-3, M-4, and M-5

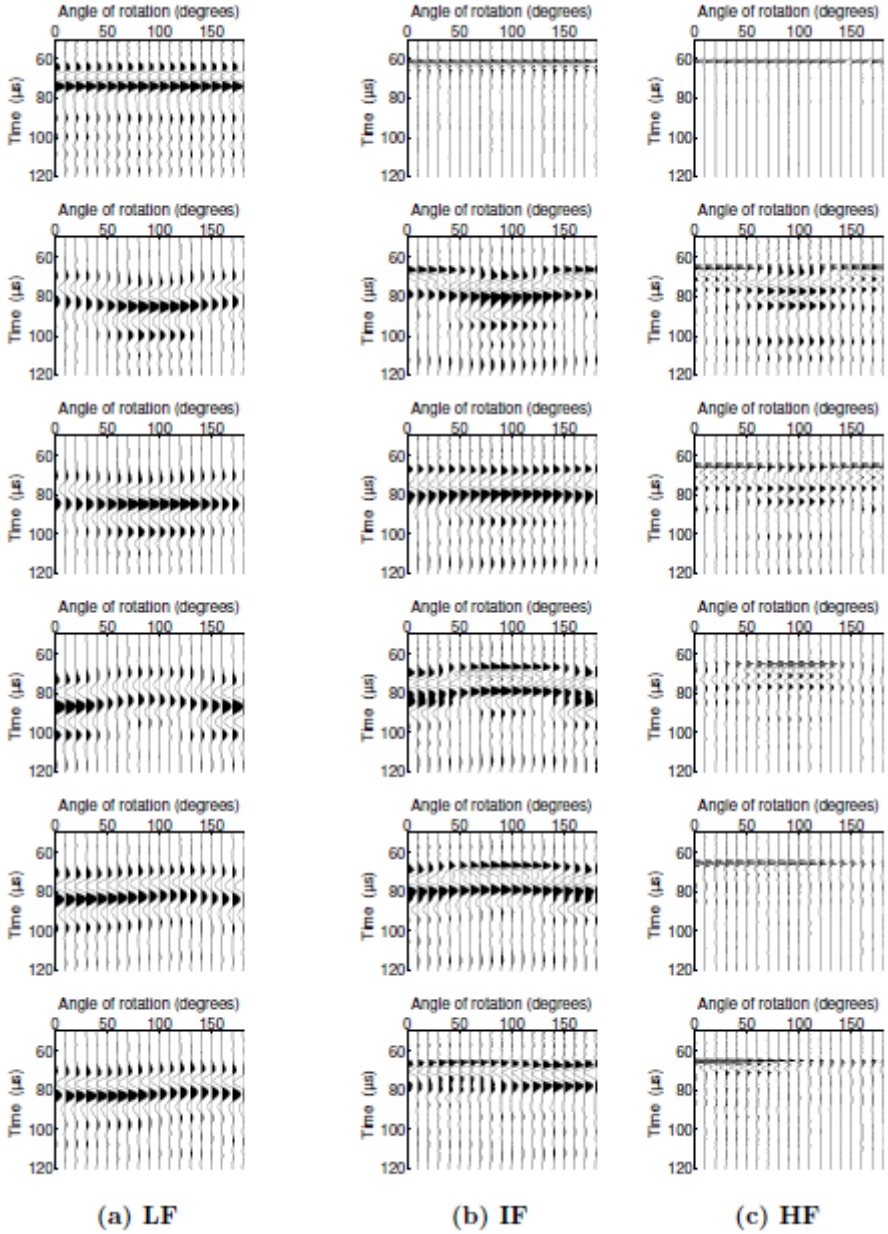

Source: The author

Figure 3.2 – S-wave seismograms for LF, IF and HF sources, as a function of change in polarization from 0° to 180°, related to propagation in Y direction. The first row corresponds to the reference (R) sample and the other rows in descending order are the seismograms for positions M-1, M-2, M-3, M-4, and M-5

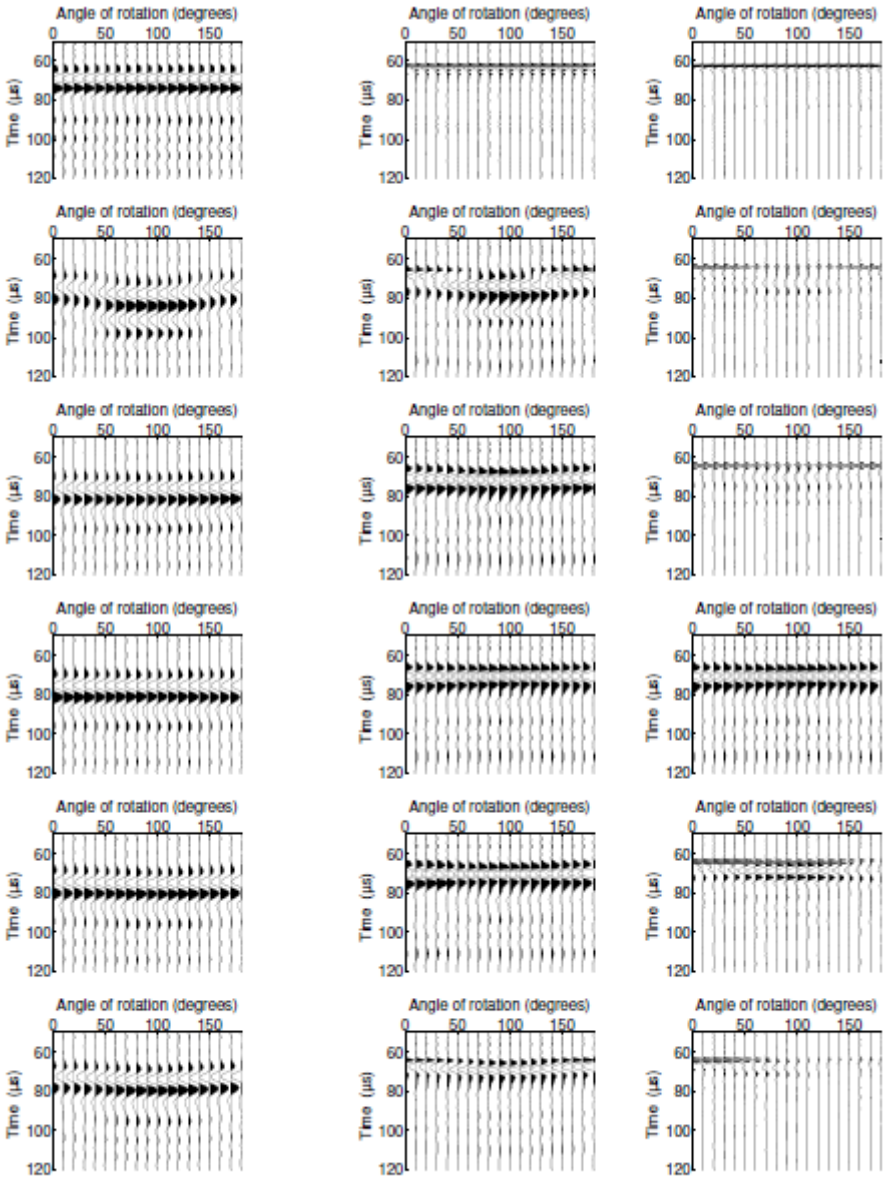

(a) LF **(b) IF** **(c) HF**

Source: The author

Figure 3.3 – S-wave seismograms for LF, IF (filtered) and HF (filtered) sources, as a function of change in polarization from 0° to 180°, related to propagation in Z direction. The first row corresponds to the reference (R) sample and the other rows in descending order are the seismograms for positions M-1, M-2, M-3, M-4, and M-5

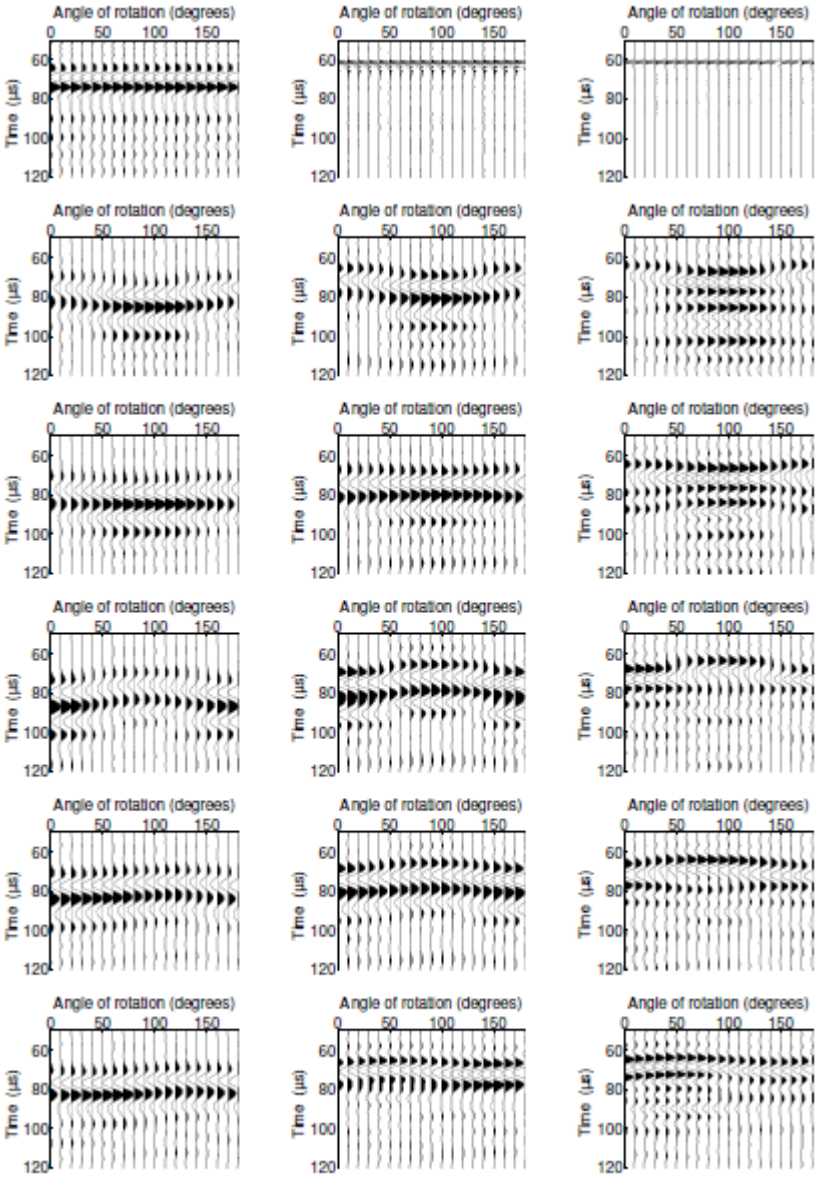

(a) LF (b) LF from IF (c) LF from HF

Source: The author

Figure 3.4 – S-wave seismograms for LF, IF (filtered) and HF (filtered) source, as a function of change in polarization from 0° to 180°, related to propagation in Y direction. The first row corresponds to the reference (R) sample and the other rows in descending order are the seismograms for positions M-1, M-2, M-3, M-4, and M-5

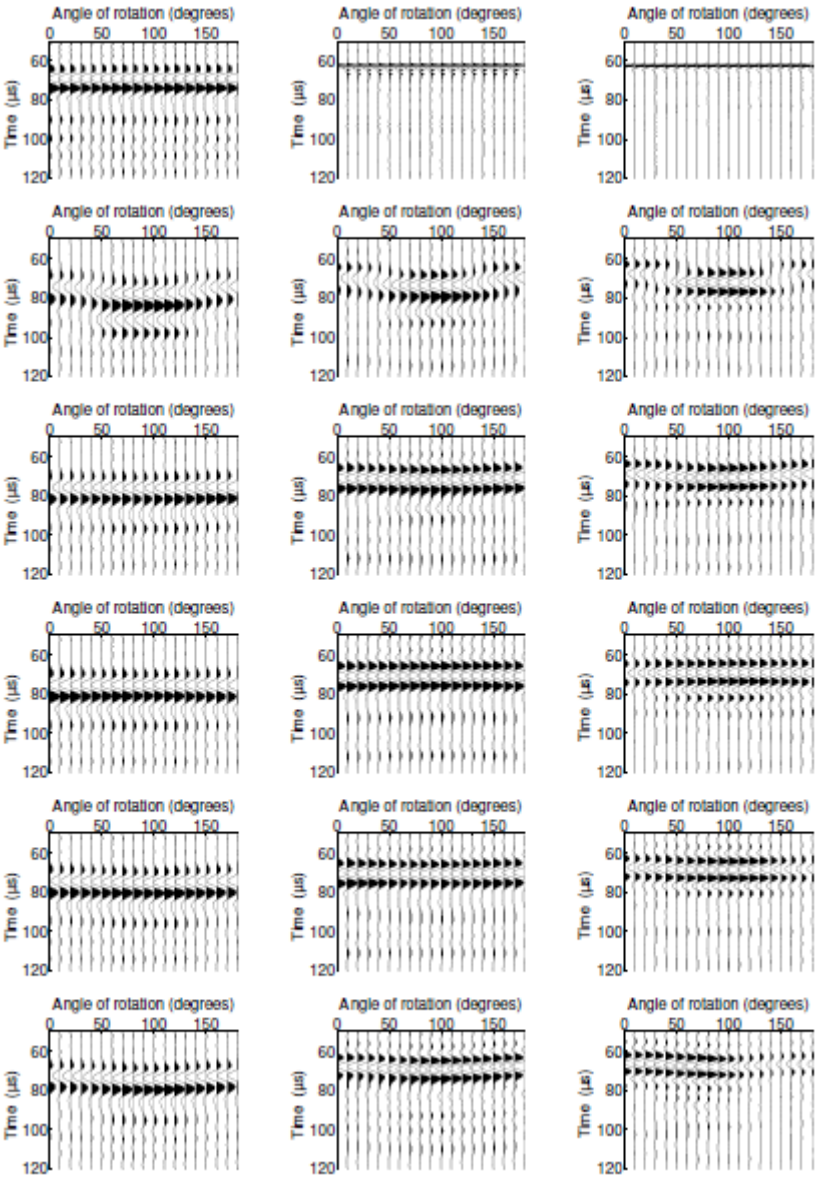

(a) LF (b) LF from IF (c) LF from HF

Source: The author

The remaining rows depict the spectrograms for wave propagation in the regions of the fractured model. It is worth mentioning that in high frequency spectrograms there are two modes of frequency distributions. One related to low frequency range and another related to high frequency range. It indicates that the attenuation of high frequency waves is more prominent than the attenuation of intermediate and low frequency waves, mainly due to scattering.

3.3 Correlogram datasets

According to Yilmaz (2001) the cross-correlation analysis measures the similarity between two different traces in time and Kennett (2002) states that cross-correlation of S-wave phases $S1(t)$ and $S2(t)$ is used to estimate S-wave polarization, θ, and time delay, δt, between these two phases. Shear-wave polarization is related to crack orientation (CRAMPIN, 1985) while the time delay is related to crack distribution (HUDSON, 1981). In this approach, the waveforms of S-wave seismograms are cross-correlated (Figures 3.1, 3.2, 3.3 and 3.4). The basic idea of the cross-correlation operation relies on two recordings, $S(\varphi, t)$ and $H(\varphi, t)$, with polarizations orthogonal to each other. These recordings are assumed to contain two orthogonal shear waves ($S1(t)$ and $S2(t)$) with the same time function, but separated in time by a delay δt. Angle φ denotes the (unknown) deviation between the trial polarizations of $S(\varphi, t)$ and $H(\varphi, t)$ from the true polarizations of $S1(t)$ and $S2(t)$. The two fundamental shear waves $S1(t)$ and $S2(t)$, the traces $S(\varphi, t)$ and $H(\varphi, t)$ can be represented by Kennett (2002)

$$S(\phi, t) = S1(t)\, cos(\phi) + S2(t + \delta t)\, sin(\phi)$$
$$S(\phi, t) = S1(t)\, sin(\phi) - S2(t + \delta t)\, \cos(\phi) \tag{3.1}$$

According to its definition [see, e.g., Yilmaz (2001)], the cross-correlation function between the two traces represented by the Equation (3.1) can be written as

$$R(\phi, \delta t) = \sum_{j=1}^{m} \sum_{i=1}^{n} S(\phi_j, t_i) H(\phi_{j+1}, t_i + \delta t) \tag{3.2}$$

where *n* is the window length (time window) of the operation (the size of trace) and *m* is the number of traces. All the correlograms described are generated correlating the first trace (0º) with each of the other traces.

First, it is analyzed the unfiltered correlograms for propagation in Z and Y direction, depicted in central and right columns of both Figures 3.7 and 3.8. They represent a mix of curves, without any clear information about fracture orientation. On the other hand, the unfiltered intermediate frequency correlograms provided more reliable information than the unfiltered high frequency correlograms.

Figure 3.5 – F-K spectra (in Z direction) related to seismograms of Figure 3.1. The Figures depicted in the first row correspond to the reference (R) sample and other rows in descending order are the spectra for regions M-1, M-2, M-3, M-4, and M-5

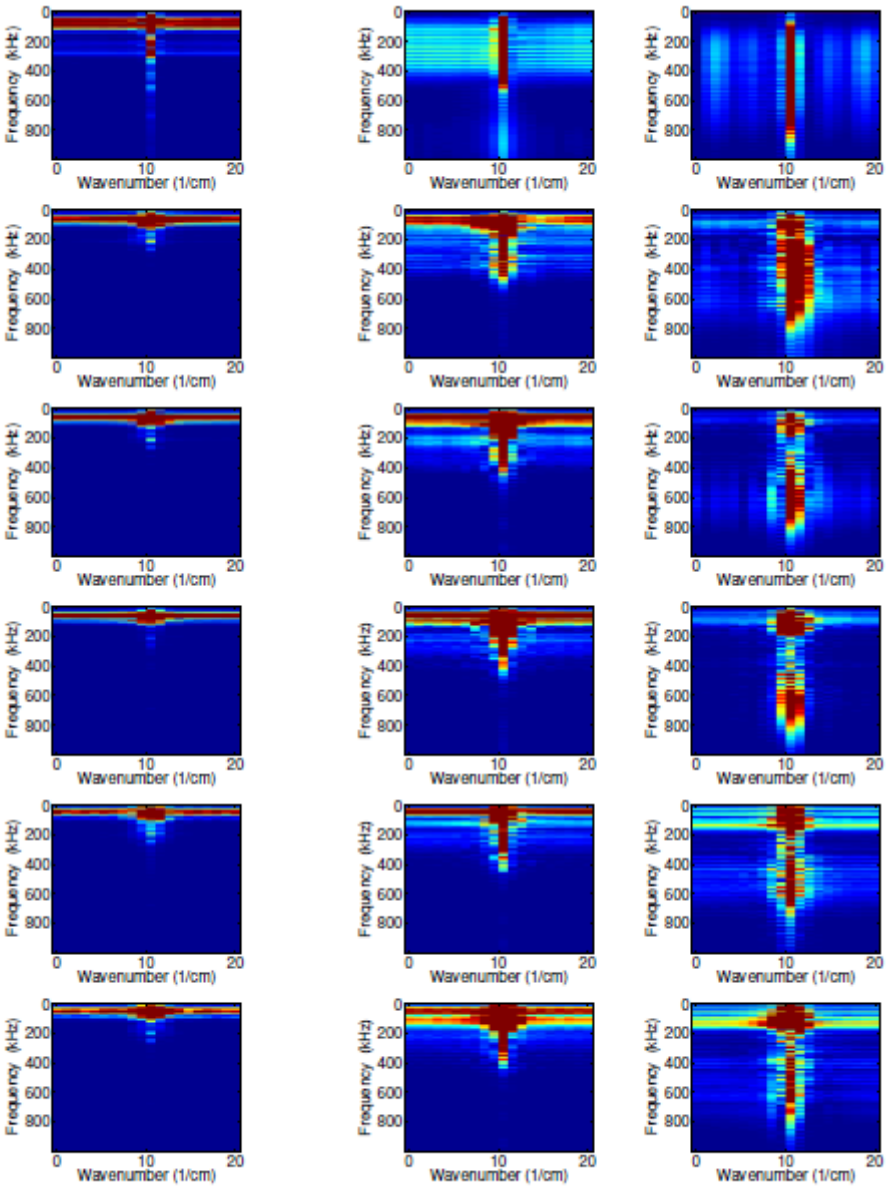

Source: The author

Figure 3.6 – F-K spectra (in Y direction) related to seismograms of Figure 3.2. The Figures depicted in the first row correspond to the reference (R) sample and other rows in descending order are the spectra for regions M-1, M-2, M-3, M-4, and M-5

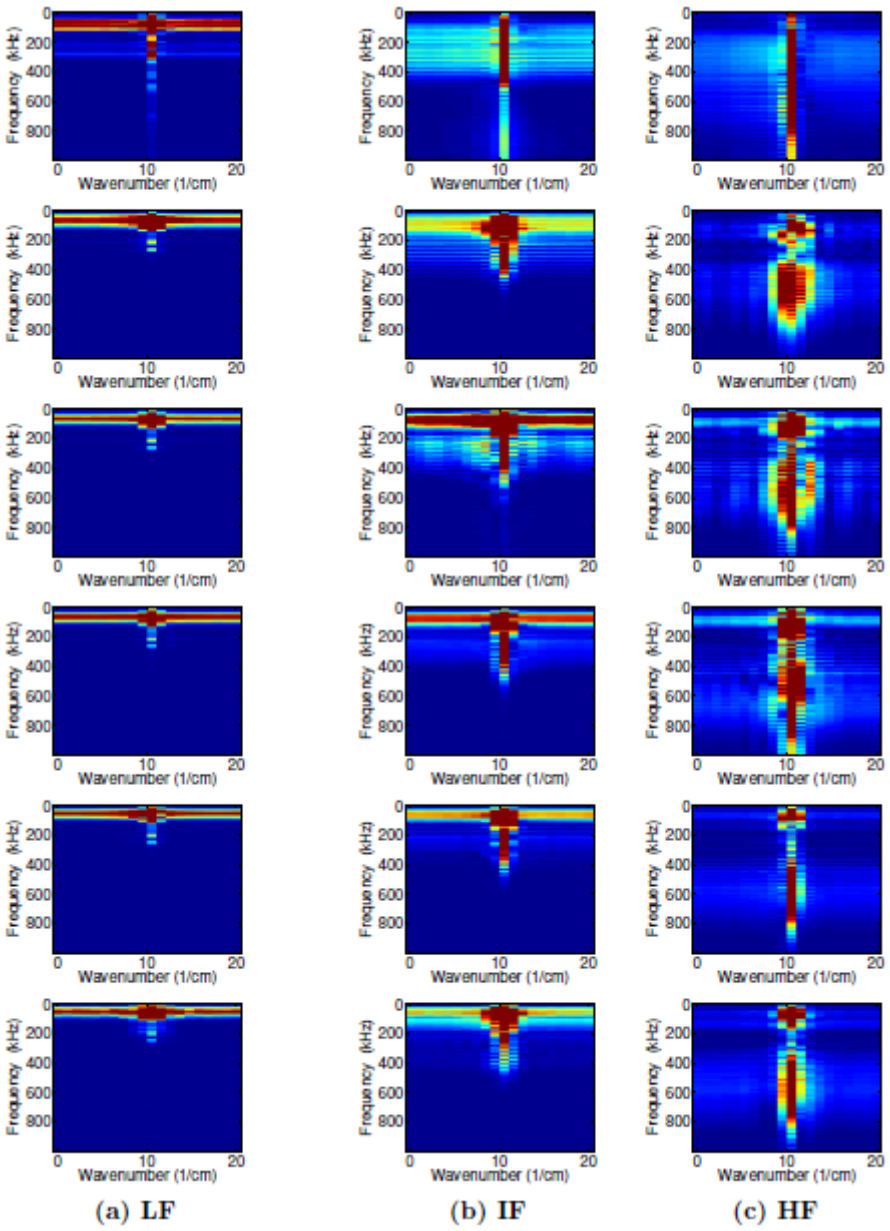

Source: The author

Figure 3.7 – S-wave correlograms related to seismograms of Figure 3.1. The Figures depicted in the first row corresponds to the reference (R) sample and the other rows in descending order are the correlograms for positions M-1, M-2, M-3, M-4, and M-5

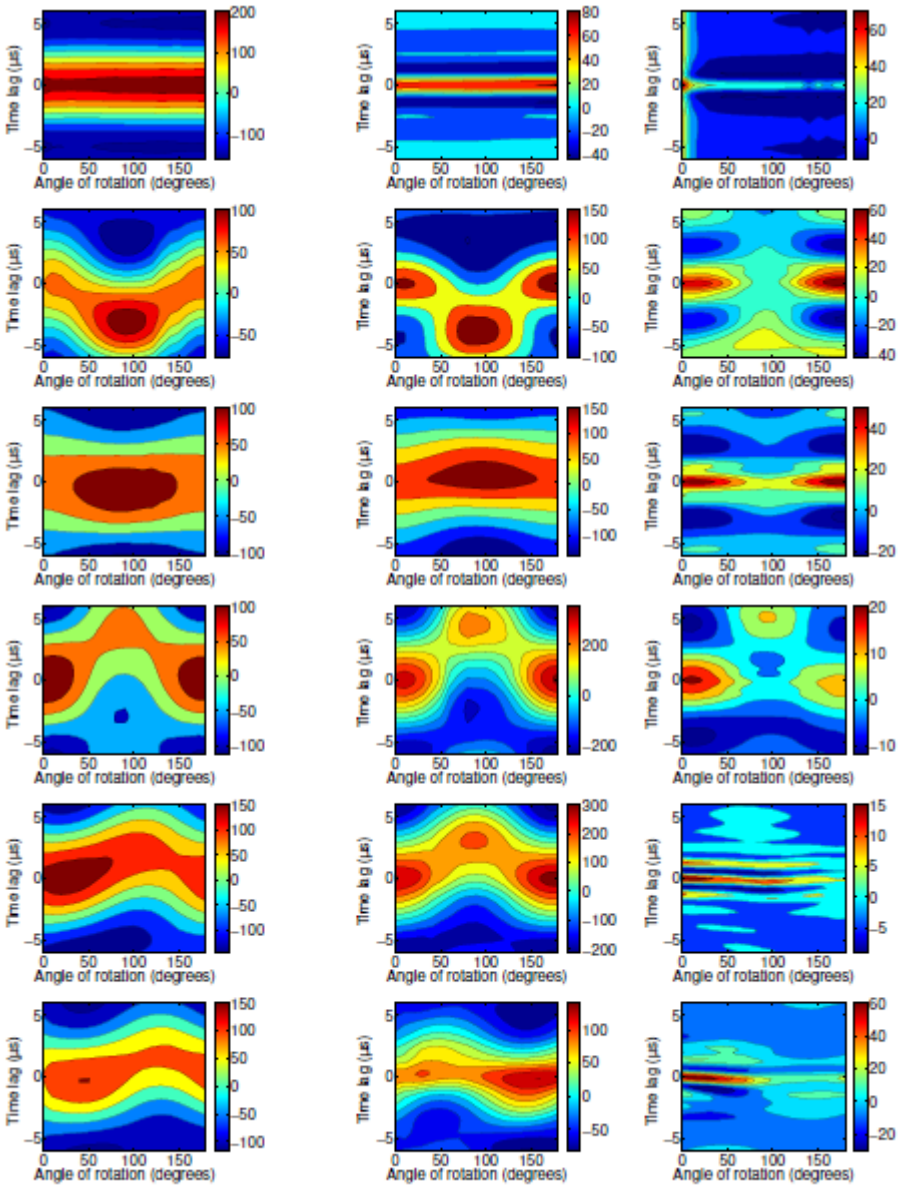

Source: The author

Figure 3.8 – S-wave correlograms related to seismograms of Figure 3.2. The Figures depicted in the first row corresponds to the reference (R) sample and the other rows in descending order are the correlograms for positions M-1, M-2, M-3, M-4, and M-5

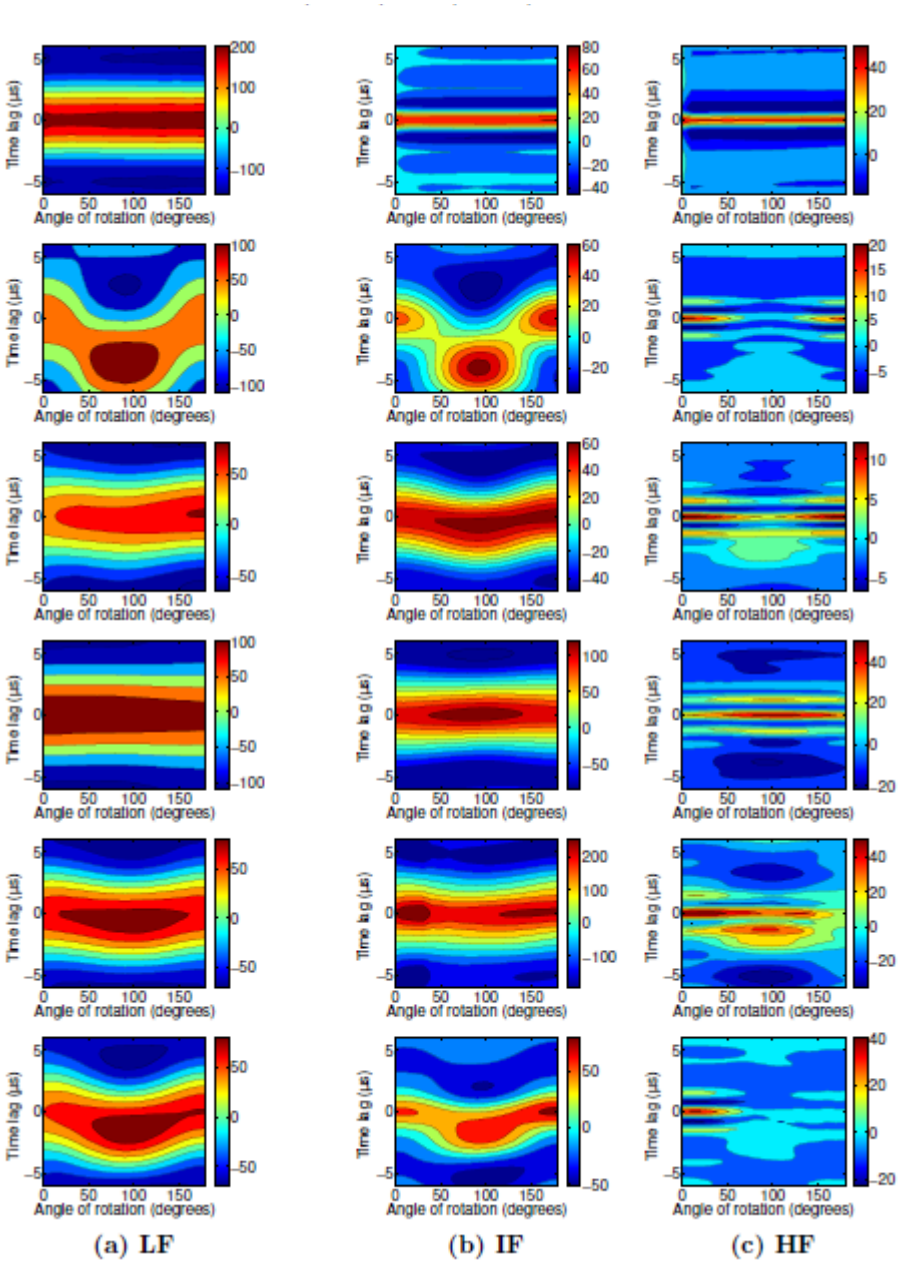

Source: The author

Figure 3.9 – S-wave correlograms related to seismograms of Figure 3.3. The Figures depicted in the first row corresponds to the reference (R) sample and the other rows in descending order are the correlograms for positions M-1, M-2, M-3, M-4, and M-5

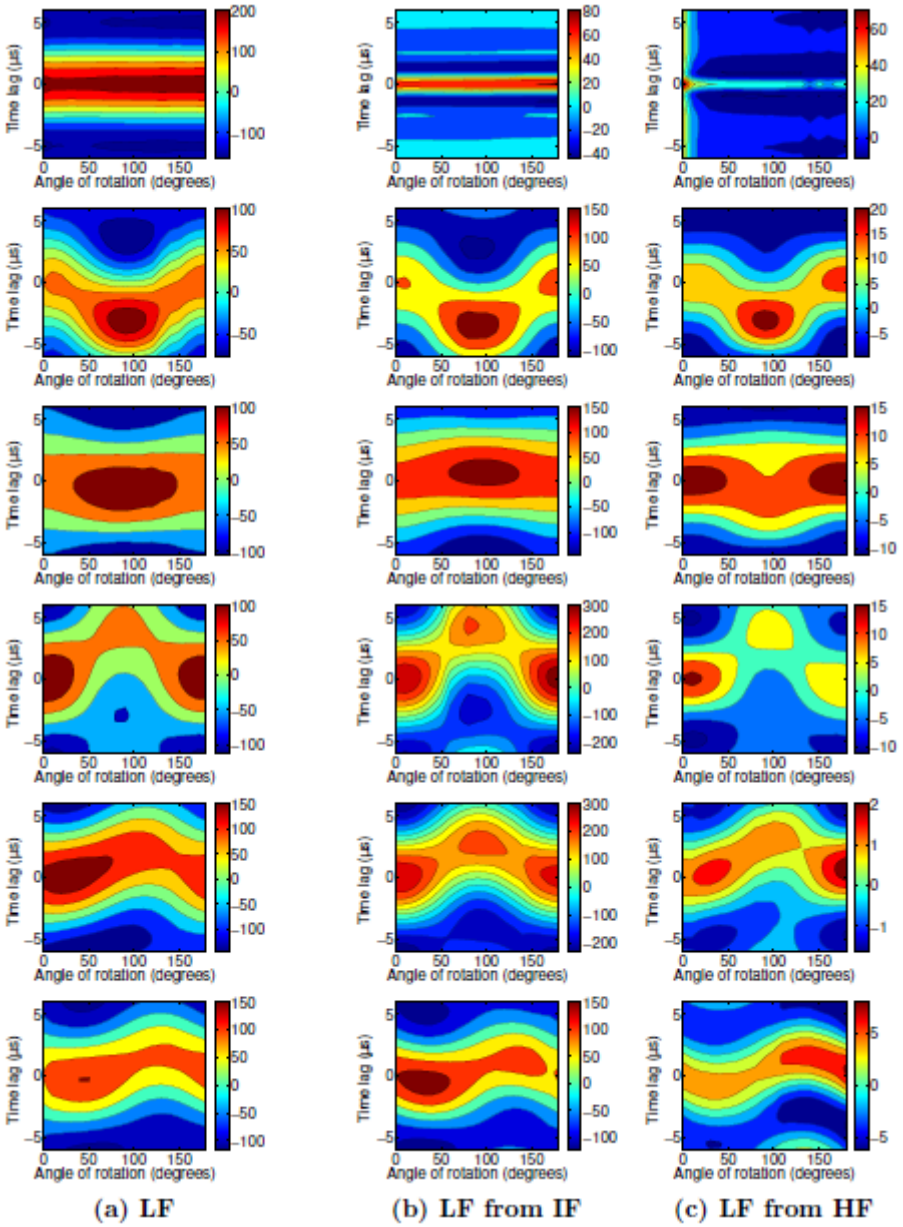

Source: The author

Figure 3.10 – S-wave correlograms related to seismograms of Figure 3.4. The Figures depicted in the first row corresponds to the reference (R) sample and the other rows in descending order are the correlograms for positions M-1, M-2, M-3, M-4, and M-5

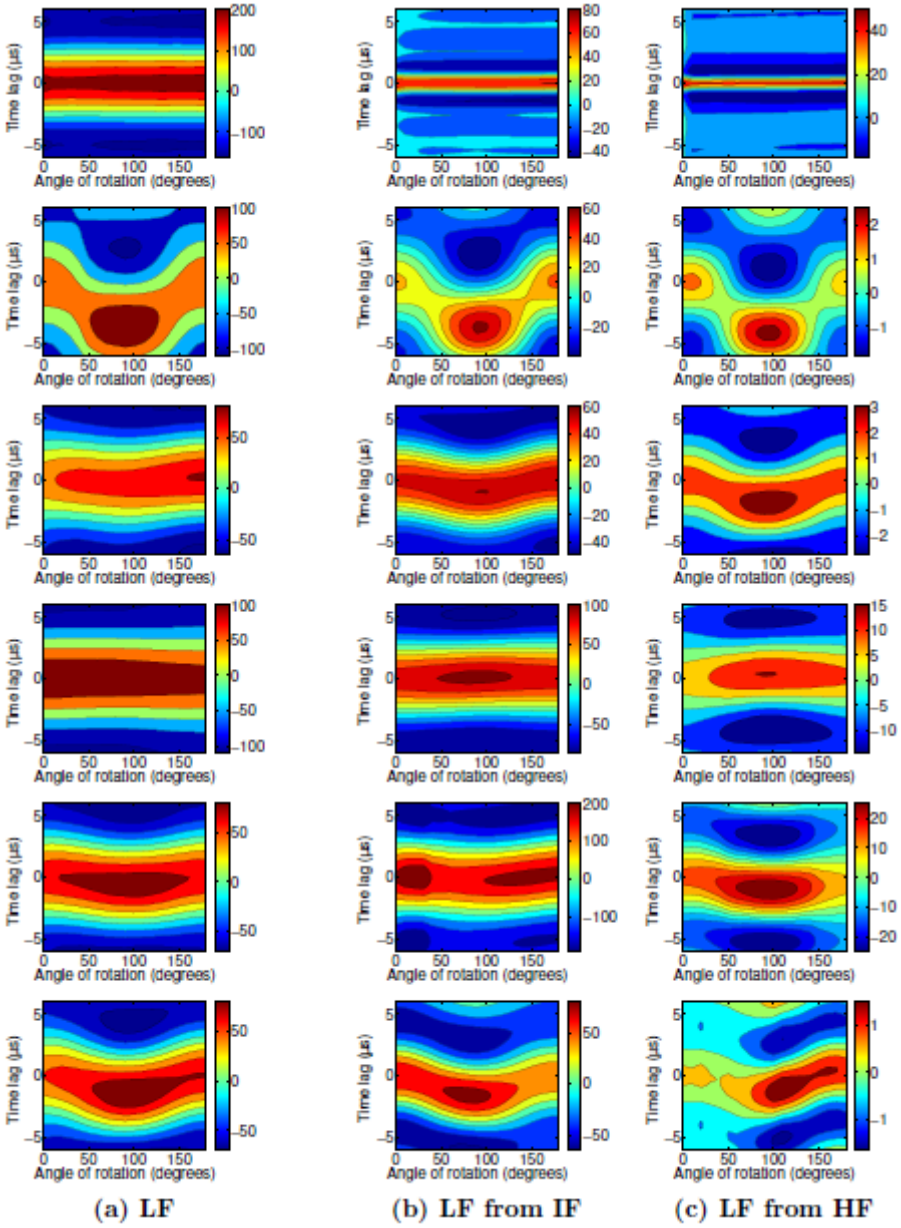

Source: The author

The figure 3.9 depicts the cross-correlation panels associated to S-wave seismograms of Figure 3.3. The correlograms in the first column are LF, while the other two columns represent the filtered data. All of them are related to S-wave propagation in Z direction. For the correlograms corresponding to the reference model in the first row, the time lag does not exist, indicating that there is no shear-wave anisotropy in the reference model.

For LF, the correlogram corresponding to region M-1 shows the highest correlation and the largest time lag of -3.2 μs at 90°. These values indicate that the fracture set is oriented at an angle of 0° parallel to X axis. In region M-3, it is identified a local correlation maximum at 90°, with a time lag of 4.4 μs. It indicates that the fracture set orientation in region M-3 is in an angle of 90° with the X axis. For region M-5, it is observed a maximum correlation value at 45°, with low negative time lag. Also, it can be observed a maximum local correlation at around 135°, which is the 90° rotated from 45°. Although the time lag amplitude is small for these directions, from the polarization it can be inferred that the fracture orientation in region M-5 is at around 45° related to the X axis. Correlation panel for region M-4 shows two local maxima, one at 20° and the other one at 100°. They do not have coherence in their polarization. Analyzing the existing small time lag, it is not possible to infer anything about the orientation in this region. In correlograms corresponding to region M-2, it is stated that the time lag is almost absent. These small time lags do not provide any information about the fracture set orientation in this region.

For filtered high and intermediate frequencies, the correlograms corresponding to the region M-1 show maximum correlation at 90°. The largest time lag is -3.6μs for filtered intermediate and -3.2μs for filtered high frequency correlogram. Taking a looking at these values, it can be concluded that the fracture set orientation in region M-1 is parallel to the X axis. Filtered correlograms in region M-3 show well-defined local maximum correlation values. For filtered intermediate frequency, the local correlation maximum occurs at 80°, with a maximum time lag of 4.4μs. For filtered high frequency, the maximum time lag of 4.4μs occurs at 90°, where the local correlation maximum is located. Thus, it is inferred that the fracture set orientation in region M-3 is around 90°. For region M-5, both filtered correlograms showed one of the maximum correlation values at around 35°, while the other maximum is around 145°. This is incoherent information about the orientation of the region and a different result in comparison to the low frequency correlogram result. As well as for low frequency correlograms, the filtered correlograms for regions M-2 and M-4 do not show any reliable information about fracture set orientation. The Figure 3.10 shows six cross-correlation panels for each frequency range, which are associated to S-wave seismograms of Figure 3.4. Again,

the first column represents the correlograms for low frequency, while the other two columns represent the filtered data, for propagation in Y direction, and the first row depicts the reference correlograms.

In region M-1, the low frequency correlogram shows a maximum correlation value at 90° associated with a time lag of -3.6μs. This high time lag value indicates that the fracture set orientation in region M-1 is parallel to the X axis, which is the same result found for propagation in Z direction. The correlograms representing regions M-2, M-3, M-4 and M-5 show a similar pattern, with almost no time lag existing, such as the correlograms of the reference model. From these correlograms, it is not possible to conclude anything about the fracture set orientation on these regions.

For filtered correlograms, in region M-1, the two filtered panels give different results. The filtered intermediate frequency panel indicates a maximum correlation at 90°, with a maximum time lag of -3.8μs, while the filtered high frequency panel indicates the maximum correlation value at 100°, with time lag of -4.2μs. From the filtered data, it can be inferred that the fracture orientation in this region is between 90° and 100°. For regions M-2, M-3, M-4 and M-5, both filtered intermediate and high frequency panels show that all waveforms are almost well-correlated, with small time lags. The small time lags do not permit the conclusion of something about the preferential fracture orientation in these regions. From these filtered correlograms, it is not possible to conclude anything about regions M-2 and M-4.

3.4 Anisotropy parameter γ

It is well established that the Thomsen parameter γ represents how much a medium is anisotropic (THOMSEN, 1986). This parameter is related to the velocities of the orthogonal shear-waves polarizations, S1 and S2. In this work, it is used the same notation for γ as described in Thomsen (op.cit.)

$$\gamma = \frac{C_{66} - C_{44}}{2C_{44}} = \frac{1}{2}\left(\frac{V_{S1}^2}{V_{S2}^2} - 1\right) \tag{3.3}$$

where $C_{66} = \rho V_{S1}$ and $C_{44} = \rho V_{S2}$ are elastic stiffness coefficients and ρ is the model density. The density here is absent in Equation (3.3) because the density model is always constant. Rewriting the Equation (3.3) as function of $S1$ and $S2$ traveltimes

$$\gamma = \frac{1}{2}\left(\frac{\left(\frac{\Delta L}{t_{S1}}\right)^2}{\left(\frac{\Delta L}{t_{S2}}\right)^2} - 1\right) = \frac{1}{2}\left(\frac{t_{S2}^2}{t_{S1}^2} - 1\right) \tag{3.4}$$

where ΔL is the distance traveled by S-wave from the source to the receiver positions. This distance is the same for *S*1 and *S*2 polarizations.

Equation 3.4 shows that γ is given by the ratio between t_{S2} and t_{S1}, which are the highest and lowest traveltimes possible observed in a fractured medium, respectively. In this work, it is used traveltimes for different polarization angles in order to determine the preferential fracture orientation in a region. The traveltimes used were automatically extracted and associated to the highest amplitude of the signal (the first lobules of the wavelet). The equation used is given by,

$$\Gamma(\theta) = \frac{t(\theta + 90°)}{t(\theta)} \tag{3.5}$$

where θ is the polarization angle which varies from 0° to 180°. The highest value found should occur when the polarization angle used is parallel to the fractures.

The Figure 3.11 represents the γ curves for low and unfiltered frequencies, for both propagations in Z and Y direction. It is stated that the unfiltered high frequency curves, for all regions, have a behavior similar to the reference curve. This situation occurs because the wavelength of these high frequency waves is very small, even smaller than the fractures, making these waves insensitive to the anisotropy caused by the fractures. It is not possible to conclude anything about fracture orientation using these high frequencies curves. On the other hand, the intermediate frequency curves show suitable results, even without the filter, but in some situations it is difficult to extract reliable information from them.

The left column of Figure 3.12 represents the γ curves for low and filtered frequencies, for wave propagation in Z direction. At regions M-1 and M-3, the low frequency curves have a symmetric behavior, with large positive and negative amplitudes. This is an indicator that the fracture set orientations at the regions are perpendicular to each other. In addition, the zero crossing of the curves is approximately at 45°. Knowing that the largest value of γ in region M-1 occurs when the angle of rotation is 0° and the largest value of γ in region M-3 occurs when

the polarization is at an angle of 90°, it is concluded that the fracture set orientation in regions M-1 and M-3 are parallel to the X and Y directions, respectively. At regions M-2, M-4 and M-5, it is noticed that the graphics have considerable low amplitude. It is not possible to infer anything from these curves.

For filtered intermediate and high frequencies, in region M-1, both curves are similar to each other. The filtered curves have a more symmetric pattern in comparison to the curve of low frequency source, being possible to extract a more confident result from them. They have largest γ values at 0° and, at approximately 45°, the γ values are zero. It is noticed that the fracture set orientation in region M-1 is parallel to the X axis. In region M-3, the filtered curves show suitable results. The filtered high frequency curve has more prominent amplitude than the low frequency curve, while the filtered intermediate frequency curve has similar amplitude and shape than the low frequency one. Both curves have highest values at the angle of 90° and zero value at 45°. That being said, the fracture set orientation at M-3 is 90° with the X direction. For regions M-2, M-4 and M-5, the low amplitude of both filtered high and intermediate frequencies made it impossible to draw a conclusion about the fracture orientation in these regions.

The right column of Figure 3.12 represents the γ curves for low and filtered frequencies, from S-wave propagation in Y direction. On region M-1, the curve shows a symmetric behavior, with large amplitude, indicating that there is a preferential orientation of the fracture set in the region. The largest value of γ occurs at 0° and the zero crossing is at 45°, indicating an orientation of the fracture set along the X axis. The analysis of the curve on region M-3 indicates that the region is isotropic, since the γ values are very close to zero. This result is very different in comparison to the one extracted from the curves associated with S-wave propagation in Z direction. This might be explained by the alignment of the fractures in the region. At regions M-2, M-4 and M-5, the curves have considerable low amplitude, making it impossible to extract clear and reliable information from them.

The filtered curves corresponding to region M-1 show considerable high amplitudes. The filtered high frequency curve shows a rectilinear behavior, while the filtered intermediate curve shows a sinusoidal behavior. Although they have different shape, both have a symmetric behavior and high amplitude, which indicates a preferential orientation in the region. The maximum γ value at 0° indicates a fracture orientation along the X axis in the region. From the remainder curves, it is not possible to infer anything about the fracture orientation since they all have considerable low amplitude and most of them are completely non-symmetric.

Figure 3.11 – Anisotropy parameter curves for low frequency and intermediate and high frequencies unfiltered. Figures depicted in the first row corresponds to the reference (R) sample and other lines in descending order correspond to curves for positions M-1, M-2, M-3, M-4, and M-5. First column corresponds to the curves associated to S-wave propagation in Z direction while the second column corresponds to S-wave propagation in Y direction

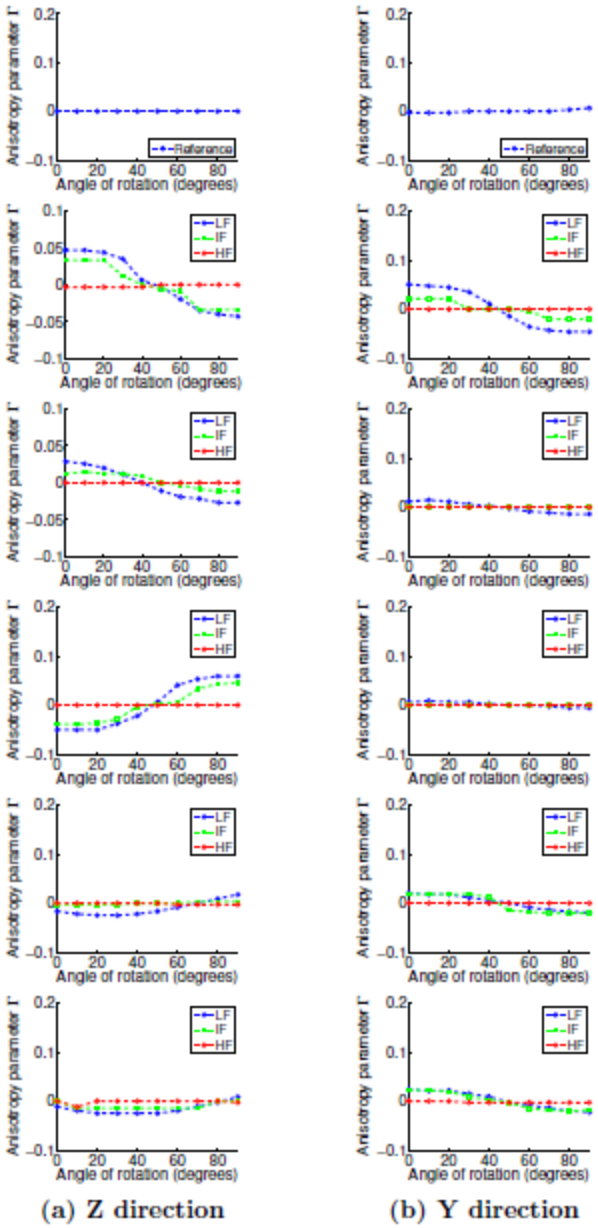

Source: The author

Figure 3.12 – Anisotropy parameter curves for original low frequency and intermediate and high frequencies filtered. Figures depicted in the first row corresponds to the reference (R) sample and other lines in descending order correspond to curves for positions M-1, M-2, M-3, M-4, and M-5. First column corresponds to the curves associated to S-wave propagation in Z direction while the second column corresponds to S-wave propagation in Y direction

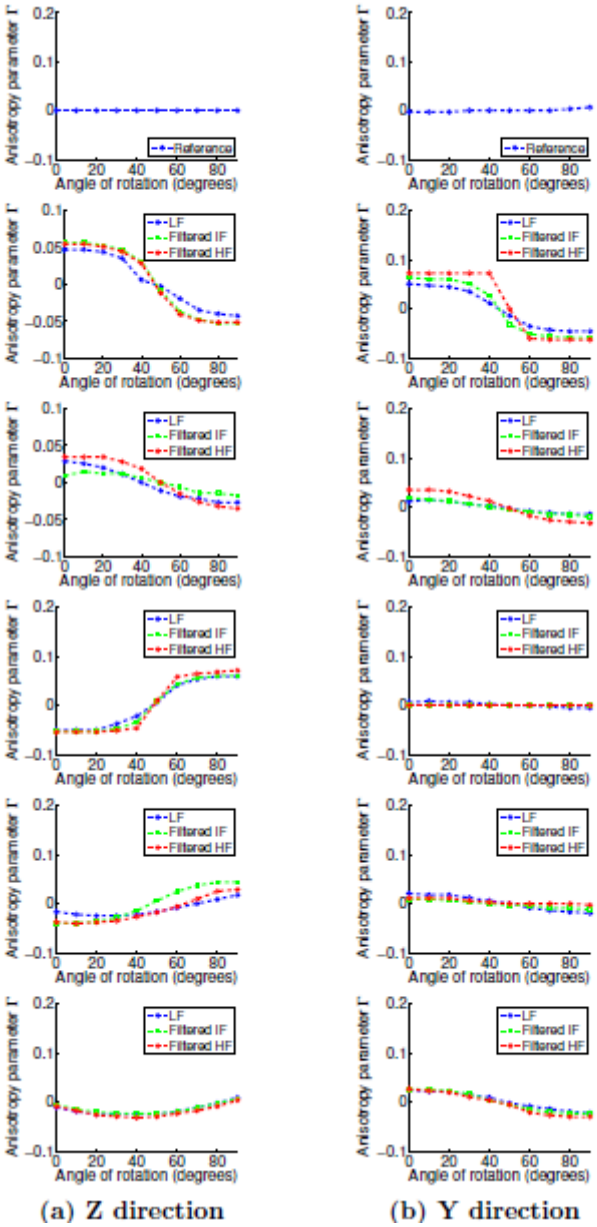

Source: The author

Figure 3.13 – Source frequency versus anisotropy parameter low and filtered frequencies. The Figures are depicted from position M-1 to position M-5, in descending order. The first column corresponds to S-wave propagation in Z direction while the second corresponds to S-wave propagation in Y direction

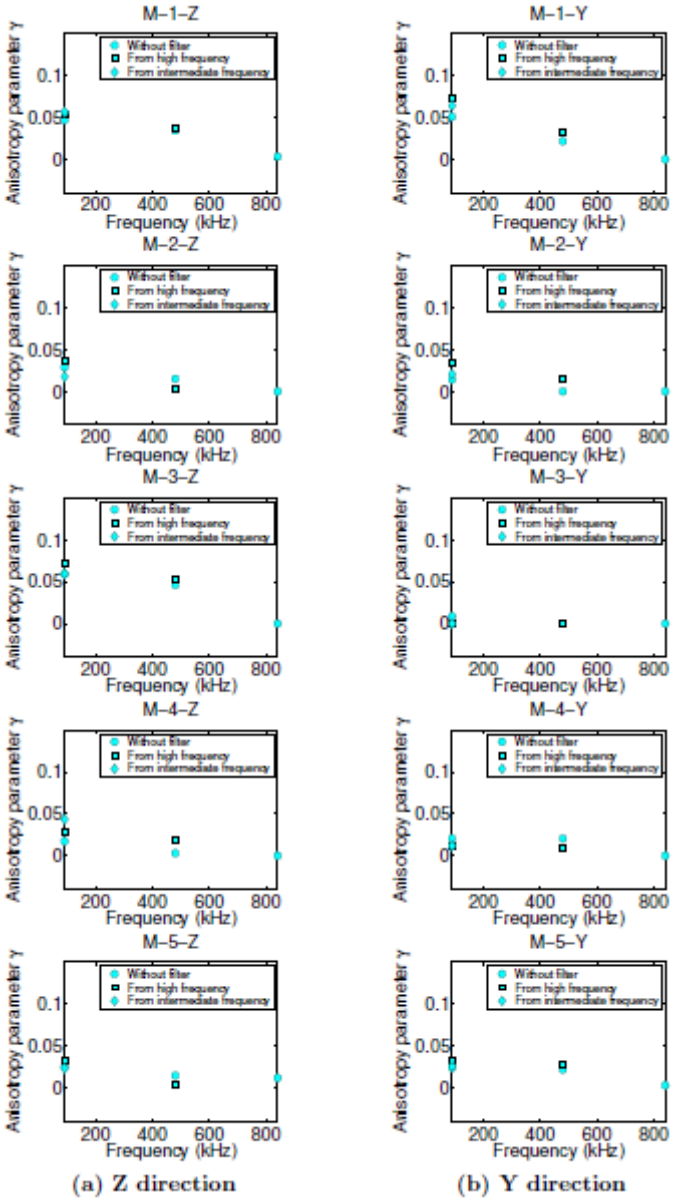

Source: The author

3.5 Frequency attenuation

In most natural materials, seismic attenuation increases with frequency (QUAN AND HARRIS, 1997). If the fractures and fracture spacing are close in size to the seismic wavelength, the fractures will scatter the seismic energy causing a complex seismic signature or coda (WILLIS et al., 2005). According to Figueiredo, Schleicher e Stewart (2013), the S-wave phase propagating with polarization perpendicular to a fracture suffers a bigger attenuation in comparison to the S-wave phase propagating with polarization parallel to the same fracture, i.e., the faster S-wave (S1) is less attenuated than slower S-wave (S2). In this approach, it is used high frequency waves, with 840 kHz, to estimate the fracture orientation in a medium from the analysis of scattering waves. First, the Fourier transform is calculated in each signal of the high frequency seismograms, corresponding to each angle of rotation. This process is repeated for each region of the model, from M-1 to M-5, for both Z and Y direction. Analyzing the amplitude spectrum of each trace, the maximum amplitude value of the higher frequencies is picked, which represent the scattered energy. To each amplitude picked, it is defined the corresponding frequency. This process is repeated for each angle of rotation. Knowing these values of frequency, a graphic showing the variation of dominant frequency with the angle of rotation is generated, for S-wave propagation in Z and Y directions (Figure 3.14). In these graphics, the higher dominant frequency values represent high wave scatter, i.e., represents regions where the polarization is normal to the fractures; the lower values represent the opposite thing.

Figure 3.14 – Frequency as function of angle of transducer rotation (polarization) curves. The figures depicted in the first line correspond to the reference (R) sample and other lines in descending order are the curves for positions M-1, M-2, M-3, M-4, and M-5. The first column corresponds curves related to S-wave propagation in Z direction while the second corresponds to curves related to S-wave propagation in Y direction

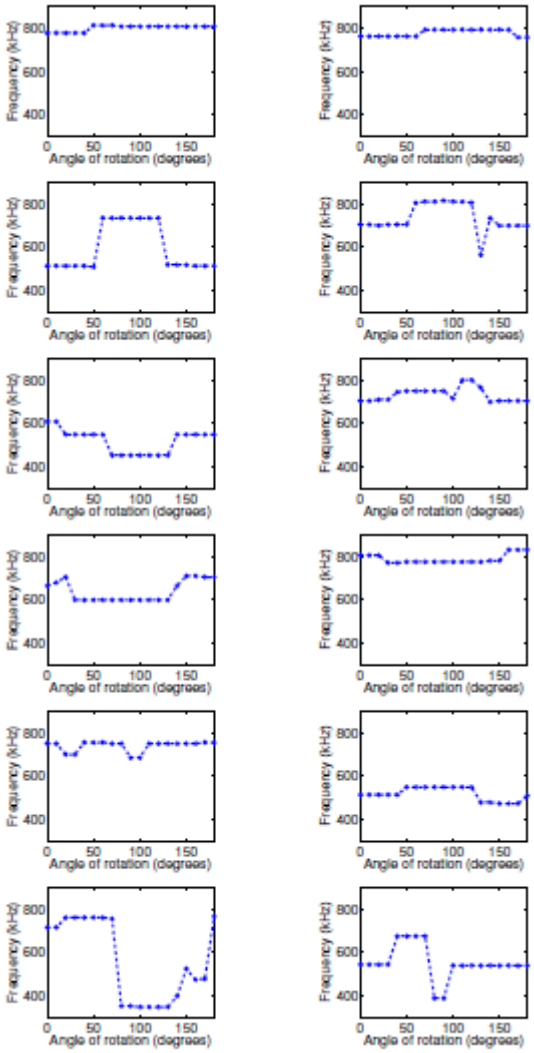

(a) Z direction (b) Y direction

Source: The author

For S-wave propagation in Z direction, in the left column of Figure 3.14, it is noticed a pattern with well-defined high and low values of dominant frequency on the graphic that corresponds to region M-1. The analysis of both highest values and lowest values allows the determination of the fracture set orientation in region M-1 is either in the range of 0° to 30° or 150° to 170° with the X axis. For S-wave propagation in region M-3, the curve related to Z direction showed an opposite behavior in comparison to the curve for region. From this conclusion it is inferred that region M-3 should have fracture orientation perpendicular to M-1. The graphic corresponding to region M-5 has a sinusoidal pattern, with very high amplitudes, different from the previous results, making it possible to conclude that the fracture set orientation is not parallel or perpendicular with the X axis. The highest values of the graphic, which run from 0° to 70°, suggest a preferential fracture orientation between 90° and 160° with the X axis. From the lowest values of dominant frequency, which have close values, a preferential fracture orientation between 80° and 140° is inferred, which is inside the range found from the highest values. The interpretation of both highest and lowest values in the graphic determines that the preferential orientation of the fractures in region M-5 is within the range between 90° and 160°. The curves for regions M-2 and M-4 show small amplitudes in comparison to the other curves, which is an indicative that there is no preferential orientation in these regions.

The right column of Figure 3.14 shows the graphics of attenuation associated to seismograms obtained from the Y direction. The curve representing region M-1 shows the same shape of the one in region M-1 for propagation in Z direction (see the second row), but with a smaller amplitude. Even with this smaller amplitude it is possible to state, from this curve, that the fracture orientation in this region is inside the range between 0° and 30° or 150° and 170° with the X axis. Related to Y direction, M-3 showed a linear behavior. It can be concluded that the inclusions have an isotropic homogenous distribution in this region. In other words, the orientation of fractures is parallel to the Y axis. For region M-5, despite the smaller amplitude compared with the curve from the same region but in the Z direction, the curve showed the same shape. This indicates that orientation of cracks in this region is inside the range between 80° and 90° or between 130° and 160° with the X axis .For regions M-2 and M-4, an almost linear behavior of frequency versus angle of rotation curves is perceived. So, it can be inferred that this regions are transitions zones.

4 DISCUSSION

From the low frequency seismograms, it was able to infer the fracture orientation only for regions M-1 and M-3, because of the visible time lag between the waves of 0° and 90° in both seismograms (for S-wave propagation in Z direction). In regions M-2, M-4 and M-5, the time lag is less prominent than the time lag in regions M-1 and M-3, providing a less accurate interpretation for these regions. For S-wave propagation in Y direction, with the exception of seismogram associated to region M-1, the seismograms present almost no visible time lag, not allowing the extraction of information from them.

The results obtained with cross-correlation and Thomsen parameter, for low frequency provided the best results when the data was obtained for S-wave propagating perpendicular to the bedding planes. For this direction of propagation, these two techniques showed suitable agreement with each other. They correctly identified the preferential fracture orientation in regions M-1 and M-3.

For region M-5, it was only possible to extract information about fracture orientation from the correlogram, while the curves presented uncertain information. The clear results in regions M-1, M-3 and M-5 extracted from the correlograms and the unclear information in regions M-2 and M-4 indicate that M-2 and M-4 are transition zones. These techniques described showed uncertain results for most of the regions when the S-wave propagation was in Y direction.

The use of transducers with different sizes gives different results in the estimative of anisotropic parameters (LI; OKOYE; UREN, 2000). In this work, this concept was not used, but it is showed that different frequencies give different information about the anisotropic parameters. Also, it is verified, from the spectrograms, that high frequency waves suffer more attenuation due to the fractures in the model than the lower frequencies. Based on this high degree of attenuation suffered by high frequency waves, it was possible to estimate the fracture orientation in the regions of the model from the analysis of the graphics in Figure 3.14. The results extracted from these curves were purely qualitative.

The biggest contribution of the attenuation graphics are the definition of the regions. It is explicit with the analysis of the graphics for propagation in Z direction that there are five different well-defined regions. The prominent amplitudes in regions M-1, M-3 and M-5 for propagation in Z direction allows only the definition of qualitative values of fracture orientation, but it is an indicative that the fractures in these regions have different disposal,

while the fractures in regions M-2 and M-4 are transition zones. Moreover, the graphic for propagation in Y direction was the unique capable of extract information when the S-wave propagation was parallel to the bedding plane.

The recovering of low frequency signal, by filtering higher frequency signals, provided satisfactory results. The error graphic (Figure 3.13) depicted that the error between low frequency and filtered data was small, within a margin of error. All the filtered seismograms, curves and the filtered correlograms showed suitable results in comparison to the low frequency data. From this agreement, is possible to obtain well-fitted results from filtered signals, without a significant loss of information. In some situations, as in some with curves, the result obtained with filtered data was even more satisfactory than the result obtained with low frequency data.

5 CONCLUSIONS

The analysis performed by Figueiredo, Schleicher e Stewart (2012) has been extended in order to find fracture orientation in an anisotropic medium with different fracture orientations. The analysis of S-waves velocity and frequency was used in order to recover information about the fracture set orientation in a cracked physical model. From the seismograms, it was generated cross-correlation panels, anisotropy parameter curves and frequency response curves that helped in this goal. Integrating the results of these techniques, the estimative of some characteristics of the model was possible.

Among these techniques, it was observed that the correlograms and frequency versus angle of rotation curves were the more confident on identifying transition zones. Moreover, the high frequency attenuation based curves were the only technique able to provide information about fracture orientation in region M-5 for S-wave propagation parallel to the bedding plane. This technique can be a possible tool in order to solve this problem. Although the results for the analysis of these curves were purely qualitative in fracture orientation estimative, the use of higher frequencies in future studies will probably recover more quantitative information.

This work showed the importance of the use of high frequency sources, which can give information about fracture orientation from both filtered and unfiltered signals. Moreover, the disposal of cracks in region M-3 causes an isotropic behavior in the curves and panels when the S-wave propagation is parallel to the bedding planes, causing inexact results for all the techniques implemented. When talking about the importance of developing new technologies for the characterization of fractures in subsurface, the experiment with all the techniques involved, can be used in Inter-well tomography. Also, the main contribution of this work is to show that reliable information about fracture in subsurface can be obtained from waves generated from high frequency sources.

Besides the developed analysis performed here in order to estimate fracture orientation, this work explored the use of cheap high frequency sources in order to obtain responses in lower frequency domains. From the results showed here, reliable responses were estimated for unfiltered and filtered signals.

BIBLIOGRAPHY

ASSAD, J. M.; TATHAM, R. H.; MCDONALD, J. A. A physical model study of microcrack induced anisotropy. **Geophysics**, v. 57, n. 12, p.1562-1570. 1992.

BUCKINGHAM, E. On physically similar systems: illustrations of the use of dimensional equations. **Physical Review**, v. 4, n. 4, p.345-376. 1914.

CRAMPIN, S. Evaluation of anisotropy by shearwave splitting. **Geophysics**, v. 50, n. 1, p.142-152. 1985.

FIGUEIREDO, J. J. S. de; SCHLEICHER, J.; STEWART, R. R. Estimating fracture orientation from elastic-wave propagation: An ultrasonic experimental approach. **Journal of Geophysical Research**, v. 117, n. B8. 2012.

FIGUEIREDO, J. J. S. de; SCHLEICHER, J.; STEWART, R. R. Shear wave anisotropy from aligned inclusions: ultrasonic frequency dependence of velocity and attenuation. **Geophysical Journal International**, v. 193, n. 1, p.475-488. 2013.

FAR, M. E. et al. Seismic characterization of naturally fractured reservoirs using amplitude versus offset and azimuth analysis. **Geophysical Prospecting**, v. 61, n. 2, p.427-447. 2013.

HELLER, V. Scale effects in physical hydraulic engineering models. **Journal of Hydraulic Research**, v. 49, n. 3, p.293-306. 2011.

HOLDITCH, S.; JENNINGS, J.; NEUSE, S. The optimization of well spacing and fracture length in low permeability gas reservoirs. Local: Society of Petroleum Engineers.

HUDSON, J. A. Wave speeds and attenuation of elastic waves in material containing cracks. **Geophysical Journal of the Royal Astronomical Society**, v. 64, n. 1, p.133-150. 1981.

HUGHES, S. A. Physical models and laboratory techniques in coastal engineering: **World Scientific**. 1993.

KENNETT, B. L. N. The seismic wavefield: interpretation of seismograms on regional and global scales. **Cambridge University Press**. 2002. v. 2.

KLINE, S. J. Similitude and approximation theory. Springer London, Limited. 2011.

LI, R.; OKOYE, P.; UREN, N. A study of the effects of transducer size on physical modeling experiments for recovering anisotropic elastic parameters. **Geophysical Research Letters**, v. 27, n. 22, p.3643-3646. 2000.

LONERGAN. L. Fractured reservoirs: Geological Society of London. 2007.

NELSON, R. Geologic analysis of naturally fractured reservoirs. **Gulf Professional Publishing**. 2001.

OMOBOYA, B. et al. Uniaxial stress and ultrasonic anisotropy in a layered orthorhombic medium. Local: Society of Exploration Geophysicists, 2011. p.2145-2149.

QUAN, Y.; HARRIS, J. M. Seismic attenuation tomography using the frequency shift method. **Geophysics**, v. 62, n. 3, p.895-905. 1997.

SACCHI, M. D.; VERSCHUUR, D. J.; ZWARTJES, P. M. Data reconstruction by generalized deconvolution. Local: Society of Exploration Geophysicists, 2004. p.1989-1992. 2004.

STEWART, R. R. et al. Physical modeling of anisotropic domains: Ultrasonic imaging of laser-etched fractures in glass. **Geophysics**, v. 78, n. 1, p.D11-D19. 2013.

THOMSEN, L. Weak elastic anisotropy. **Geophysics**, v. 51, n. 10, p.1954-1966. 1986.

TILLOTSON, P. et al. Experimental verification of the fracture density and shear-wave splitting relationship using synthetic silica cemented sandstones with a controlled fracture geometry. **Geophysical Prospecting**, v. 60, n. 3, p.516-525. 2012.

WILLIS, M. E. et al. 2005. Spatial orientation and distribution of reservoir fractures from scattered seismic energy: Technical report, Massachusetts Institute of Technology. Earth Resources Laboratory. (Shortened title: Fracture characterization from coda waves).

YILMAZ, O. Seismic data analysis: Processing, inversion, and interpretation of seismic data. **SEG Books**. 2001.

ZHANG, Y. et al. F-K characteristics of the seismic response to a set of discrete parallel fractures: technical report. Massachusetts Institute of Technology. Earth Resources Laboratory. (United States. Dept. of Energy (award number DE-FC26- 02NT15346)).

APPENDICES

APPENDICES A– PHYSICAL MODELING SIMILARITIES

Generally speaking, the scale effect of a specific phenomenon (in this case a geologic phenomenon) increases according to the following scale ratio or scale factor (HUGHES, 1993; HELLER, 2011)

$$\Lambda = \frac{L_{\mathrm{C}}}{L_{\mathrm{M}}} \qquad \text{(A – 1)}$$

where L_C is the characteristic length in the field while L_M is the corresponding length in the model. The inverse of the equation A - 1 is defined by 1: Λ. The size of the model, the time and the construction cost increases with the enhancement of Λ^{-1}, Λ^{-2} and Λ^{-3} (BUCKINGHAM, 1914; KLINE, 2011; HELLER, 2011). In other words, the parameter λ is related to the mechanic similarity criteria also called geometric similarity. Besides this type of similarity, other two are outstanding in the physical modeling area. The second type of similarity, called kinematic similarity, implies that there is similarity in the particles motion (velocity and acceleration) between the model and the geological structure. The third type of similarity includes the two previous types and is called dynamic similarity. This one implies that the forces acting on the model are the same acting on the geological structure.

Emphasizing what was described previously, Figure A - 1 shows illustratively how the scale change is realized through the seismic physical modeling. An anticline is used as example. In the field, this kind of structure can present sizes in the order of kilometers or hundreds of meters. Due to the limitations of physical space and budget, the reduced size of this structure is on centimeters or a few meters. In this scenario, which parameters are necessary to adjust when the interest is to investigate this type of model through physical modeling? The answer is the frequency and, consequently, the dominant wavelength in the model.

It is well-defined that the dominant frequency of a medium is directly related to the velocity of the same medium. Therefore, for the acoustic case, the velocities (V_P) in the model and in the field are given by

$$V_{\mathrm{M}} = \lambda_{\mathrm{M}} f_{\mathrm{M}} \qquad \text{(A – 2)}$$

$$V_{\mathrm{F}} = \lambda_{\mathrm{F}} f_{\mathrm{F}} \qquad \text{(A – 3)}$$

where λ_M and λ_F are wavelengths in the model and in the field, while f_M and f_F are the dominant frequencies in the model and in the field. From the equations A - 2 and A - 3 it is defined that the kinematic similarity factor between the model and the field is given by

$$\Xi = \frac{V_F}{V_M} = \frac{\lambda_M f_M}{\lambda_F f_F} \quad (A-4)$$

considering that the acoustic velocities between the model and the field can be very close to each other or sometimes equal, from the equation A - 4 it is obtained

$$f_M = \frac{\lambda_F f_F}{\lambda_M} \quad (A-5)$$

where the dominant frequency varies between 5 - 200 Hz and the wavelength can vary between 20 - 400 m. The dominant wavelength of the model, in general, varies between 0,1 - 10 cm. In the terms of magnitude, the parameters f_F , λ_F and λ_M are

$$\begin{cases} f_F \sim 10^a & \text{where } a = 1 \text{ or } a = 2 \\ \lambda_F \sim 10^b & \text{where } b = 1 \text{ or } b = 2 \\ \lambda_M \sim 10^{-2+c} & \text{where } c = 0 \text{ or } c = 1 \end{cases} \quad (A-6)$$

Therefore, equation A - 5 can be written in terms of the magnitudes of equation A - 6

$$f_M \sim 10^{[a+b-c+2]}\text{Hz} \quad (A-7)$$

which, in the case of the model, the following frequency intervals are given by

$$f_M = \begin{cases} \sim 10^4 \text{ Hz} & \text{if } a = 1, b = 1 \text{ and } c = 0 \\ \sim 10^5 \text{ Hz} & \text{if } a = 2, b = 2 \text{ and } c = 1 \\ \sim 10^6 \text{ Hz} & \text{if } a = 2, b = 2 \text{ and } c = 0 \end{cases} \quad (A-8)$$

Figure A – 1 – Physical modeling is result of distance upscale and frequency downscale from laboratory to field or verse-versa

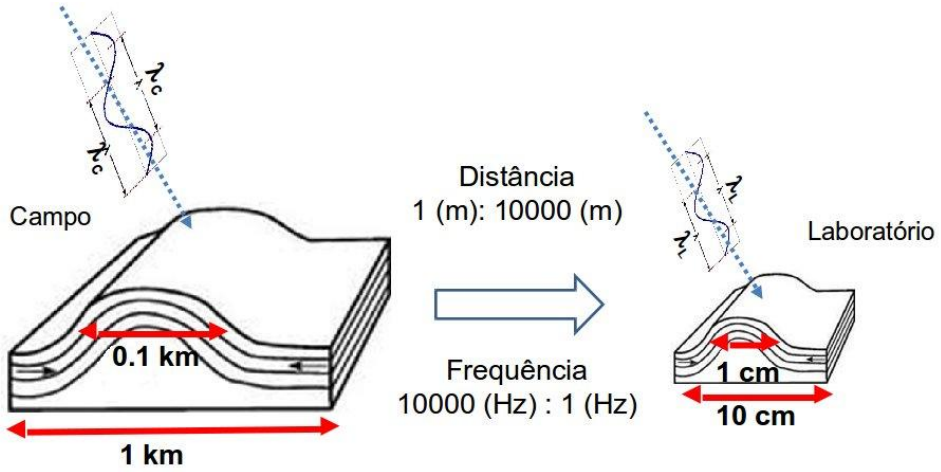

Source: Figueiredo, Schleicher e Stewart (2012)

Considering that the dominant frequencies of the ultrasonic transducers used in modeling laboratories vary between 60 kHz to 5 MHz, the first equation of system (A - 8) can be neglected .Therefore, in the field where the frequency is in an order of dozens of Hz, in the laboratory this frequency is in the order of hundreds of kHz or MHz. So, it can be affirmed that the process of physical modeling happens through an upscaling in the distance scale and a downscaling in the frequency. It is worth to say that in the case of modeling of elastic media taking into account the similarity for S-wave propagation, beyond the scale factor Ξ, another parameter related with ratio $\frac{Vp}{Vs}$ must also be considered. This case of similarity sometimes is very difficult to be reached, given the difficulty of finding materials with the same Poisson ratio of real rocks.